RSC Advances

PAPER

View Article Online
View Journal | View Issue

Cite this: *RSC Adv.*, 2021, **11**, 6934

Microphase separation/crosslinking competition-based ternary microstructure evolution of poly(ether-*b*-amide)†

Yu Wang,[ab] Zefan Wang,[b] Ping Zhu,[b] Xinran Liu,[bc] Lei Wang, *[a] Xia Dong *[bc] and Dujin Wang[bc]

The temperature dependence of the rheological properties of poly(ether-*b*-amide) (PEBA) segmented copolymer under oscillatory shear flow has been investigated. The magnitude of the dynamic storage modulus is affected by the physical microphase separation and irreversible crosslinking network, with the latter spontaneously forming between the polyamide segments and becoming the dominant factor in determining the microstructural evolution at temperatures well above the melting point of PEBA. From the rheological results, the initial temperature of the rheological properties dominated by the microphase separation (T_b°) and crosslinking (T_{cross}) structures were determined, respectively. Based on the two obtained temperatures, the microstructure evolution upon the heating can be separated into the ternary microstructure domains: homogenous (temperature below T_b°), microphase separation dominating (between T_b° and T_{cross}), and crosslinking dominating domains (above T_{cross}). When the PEBA is heated to above T_{cross}, the content of crosslinking network increases with time and temperature, leading to an irreversible and non-negligible influence on the rheological, crystallization, and mechanical properties. A more pronounced strain-hardening phenomenon during the uniaxial stretching is observed for the sample with a higher content of crosslinking network.

Received 18th December 2020
Accepted 24th January 2021

DOI: 10.1039/d0ra10627e

rsc.li/rsc-advances

Introduction

Block copolymers are composed of two or more different segments within the molecular chain, and have attracted great attention in the past few decades because of their excellent mechanical properties and processability. Depending on the architectures, block copolymers can be classified into several categories, *e.g.* (AB) di-block, (ABA) tri-block, and $(AB)_n$ multi-block (segmented) copolymers, *etc.* Due to the thermodynamic immiscibility between the segments, several long-range order structures can be formed within a sub-micrometer scale (known as microphase separation).[1–5] With extensive research, the morphology of different phases is greatly affected by the Flory interaction parameters between the two segments, composition, and the overall degree of polymerization.[6–14] Furthermore, the material properties such as modulus,[15–17] conductivity,[18,19] and rheological properties[20,21] can be enhanced at the order states. In recent decades, the order-to-disorder transition temperature and its morphology evolution of di- and tri-block copolymers have been well studied by various means such as small-angle X-ray scattering (SAXS)[2,10,21–23] and rheological technique.[2,10,20–27] Bates *et al.* have demonstrated that the viscoelastic properties of di-block copolymers are sensitive to the microstructure changes, and it can be used to characterize the morphology of ordered microstructures.[21,23–26] Hashimoto and Han *et al.* have studied the order-to-disorder transition of the polystyrene-*block*-polyisoprene-*block*-polystyrene tri-block copolymer,[2,22] and trace its microstructure evolution by the SAXS and transmission electron microscope (TEM) techniques, the results are in good agreement with that determined by rheological studies. Phase diagrams of di- and tri-block copolymers can be interpreted and predicted quite well on the thermodynamic model based on Leibler's works.[6,8]

For the segmented copolymers such as thermoplastic polyurethane (TPU),[12,20] poly(ether-*b*-amide) (PEBA),[28] poly(ester-ether) (PEE),[14] olefin block copolymers (OBC),[29] and transparent polyamide random copolymers,[30] the structure–property relationship has been widely explored in the past three decades.[7,10,30–32] Velankar and Cooper carried out a series of work to study the influence of chain architectures (including block length and block species) on the microphase separation of TPU,[12,13,33] which provides an in-depth understanding on the phase behavior of segmented copolymers. The influence of

[a]*Shenzhen Key Laboratory of Polymer Science and Technology, College of Materials Science and Engineering, Shenzhen University, Shenzhen 518060, P. R. China. E-mail: wl@szu.edu.cn*

[b]*CAS Key Laboratory of Engineering Plastics, Beijing National Laboratory for Molecular Science, Institute of Chemistry, Chinese Academy of Sciences, Beijing 100190, P. R. China. E-mail: xiadong@iccas.ac.cn*

[c]*University of Chinese Academy of Science, Beijing, 100049, P. R. China*

† Electronic supplementary information (ESI) available. See DOI: 10.1039/d0ra10627e

microphase separation on the crystallization of segmented copolymers at quiescent or flow states also has been investigated by various techniques.[28,30,34–36] It was found that the microphase separation at molten state has an effect on the morphology and size of the hard domain's crystals. Due to the co-existence nature of multi-components and multi-phase, the microstructure evolution of semi-crystalline segmented copolymer during the deformation is complicated. As the applied strain increased, the segmental chains' orientation, the crystal–crystal transition, and strain-induced crystallization can occur.[37–40] Studying the microstructural evolution under the external fields is important for a better understanding of the macroscopic properties of the segmented copolymers. To date, the phase diagram of multi-block copolymers cannot be predicated well due to the more complex segmental interactions. In other words, the phase transition temperatures and the corresponding morphologies can only be determined experimentally.

PEBA segmented copolymer, which contains the polyamide hard-segment and polyether soft-segment, has been widely used in various fields such as sports equipment, polar clothing, and medical supplies. However, the studies focused on the temperature effect on the rheological properties,[41] and crystallization morphology are limited.[35] The systematic explore the microstructure evolution upon temperature is inadequate. It was reported that the polyamide crosslinking reaction could occur at the molten state in various polyamide (PA) systems, including PA6,[42,43] PA6,6,[42–45] PA6,10,[42,43] PA11,[46] PA12,[47] and PA1012,[48] especially after prolonged heating. The polyamide crosslinking is caused by the formation of the secondary amine groups,[49] which reacts further with carboxyl groups to form the branched structures at high temperature.[50] Therefore, the influence of the formed crosslinking structure on the microstructure evolution should not be ignored for the PEBA segmented copolymers.

The present investigation aims to probe the temperature dependence on the microstructure from apparent homogenous to crosslinked states *via* the small amplitude oscillatory shear (SAOS) measurement for the commercial PEBA copolymer with the trade name of Pebax®, for which contains the crystalline hard segment of PA12, while poly(tetramethylene oxide) (PTMO) as the soft segment.[28,51] Based on the experimental results, there different microstructure domains of apparent homogenous, microphase separation, and crosslinking structure can be quantitatively determined. The influences of the microstructure on the rheological and mechanical properties is also studied by the thermal history under different temperature domains.

Experimental

Materials and sample preparation

The commercial PEBA elastomers with different compositions employed here are Pebax® 2533 SD02, 3533 SP01, and 4033 SP01 (named as P25D, P35D, and P40D in this work), supplied by Arkema Co., Ltd., used as received. The sub-grade of SD02 and SP01 has been developed to be heat and UV resistant, and the SD02 contains mould release additive. Its repeating unit is composed of the hard-segments of PA12, soft-segments of PTMO, the chain extender of adipic acid (shown in Fig. 1).[28,51] It was reported that the molecular weights of PA12 segment of P25D, P35D and P40D are 530, 674, and 800 g mol^{-1}, while the molecular weights of PTMO segment are 2000, 1870, and 1060 g mol^{-1}, respectively.[52] The average molecular weight of the PEBAX elastomers is $\sim 5 \times 10^4$ g mol^{-1}.[52] By the elemental analysis, Rezac and John[53] calculated the repeat unit numbers of PA12 ('*x*' in Fig. 1) and PTMO segments ('*y*' in Fig. 1) are 2.68 and 27.80 for P25D, also 3.42 and 26.00 for P35D, 4.06 and 14.72 for P40D. The weight fraction of PA12 segments (W_{PA}) of the studied elastomers determined by ^{1}H NMR are list in Table 1.[28,40]

The thermal properties of the three studied copolymers were determined by differential scanning calorimetry (DSC Q2000, TA instruments). The instrument was calibrated with indium before measurements. Temperature scans were performed in the range of −50 to 200 °C with a heating/cooling rate of 10 °C min^{-1} under the nitrogen atmosphere. The melting temperature (T_m), crystallization temperature (T_c), the corresponding melting and crystallization enthalpies (ΔH_m and ΔH_c) for the PA12 and PTMO crystals are denoted by the subscript "HS" and "SS", respectively. The crystallinity of PA12 crystals (X_c) was calculated by the normalized $\Delta H_{m,HS}$ with the fraction of PA12 HS dividing by the fusion enthalpy of perfect PA12 crystals (246 J g^{-1}).[40] The results are listed in Table 1.

To remove the absorbed moisture, the raw pellets were dried at 100 °C under vacuum for 12 hours. Both the thin films with a thickness of 0.5 mm and the rheological specimens with 25 mm diameter and a thickness of 1 mm were prepared by melt-pressed under 180 °C and 50 MPa for 3 min by mold, then quickly cooled to room temperature by cold compression for 3 min.

Rheological measurement

Linear viscoelastic properties of the PEBA elastomer at molten state with various temperatures were measured by a stress-controlled rheometer (DHR2, TA Instruments) with a 25 mm parallel plates feature, the gap-value was 1 mm. All the experiments were carried out under the nitrogen atmosphere to protect the samples from oxygen degradation.

The samples were heated to different isothermal temperatures (T_{iso} = 170, 190, 200, 210, 230, 250, and 270 °C), kept for 3 min to ensure all the crystals were melted, then the dynamic time sweep was performed for obtaining the time dependence of the dynamic storage modulus (G') and loss modulus (G'') within 2 hours isothermal at each temperature. To understand

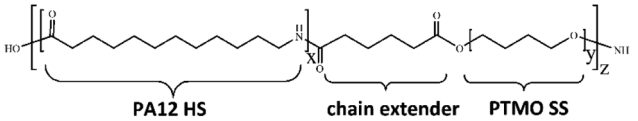

Fig. 1 General chemical structure of the studied Pebax® elastomers. The repeating numbers of PA12 HS and PTMO SS are denoted as "*x*" and "*y*", respectively.

Table 1 The thermal properties of the raw and thermal-treated PEBA copolymers

Sample		W_{PA}	$T_{c,SS}$ (°C)	$T_{m,SS}$ (°C)	$T_{c,HS}$ (°C)	$\Delta H_{c,HS}$ (J g^{-1})	$T_{m,HS}$ (°C)	$\Delta H_{m,HS}$ (J g^{-1})	X_c
P25D	Raw pellet[a]	0.27	−10.2	12.0	53.8	9.3	135.2	10.0	0.15
	Treated film[b]		−10.4	12.1	50.2	6.0	135.4	2.4	0.04
P35D	Raw pellet[a]	0.29	−11.9	9.0	68.9	14.5	145.0	14.7	0.21
	Treated film[b]		−10.7	9.2	68.5	8.9	145.2	5.9	0.08
P40D	Raw pellet[a]	0.46	−13.0	6.8	90.0	26.2	160.5	25.6	0.23
	Treated film[b]		−12.0	6.0	89.0	25.7	158.4	19.5	0.17

[a] The raw pellet of the PEBA elastomers were used as received. [b] The films were quenched from 270 °C after the 2 hours isothermal process.

the time effect on the phase state, the G' and G'' over a frequency (ω) range of 0.1–628 rad s^{-1} were measured by the SAOS mode for each sample before and after the 2 hours isothermal processes, respectively.

In order to determine the microphase separation transition temperature of P35D melt, the dynamic temperature ramp measurement at a given ω of 0.5 rad s^{-1} with various heating rates of 0.5, 1.0, 1.5, and 2.0 °C min^{-1} from 160 to 270 °C were carried out by hot nitrogen gas to control the temperature in the accuracy of ±0.1 °C. With the obtained G' and G'', the binodal (T_b) and spinodal temperature (T_s) can be determined based on the Ajji and Chopin's model.[54–56]

Fourier transform infrared spectroscopy (FTIR) measurement

The FTIR spectra of P35D films with a thickness of *ca.* 30 μm was obtained by using a Nicolet 6700 FTIR spectrophotometer (Thermo Scientific) operated in transmission mode at room temperature and equipped with an MCT detector. The spectra were collected by accumulating 32 scans with a resolution of 4 cm^{-1}.

Tensile testing

The tensile testing was conducted by using an Instron model 3365. The dumbbell shaped tensile bars (3 mm wide, 25 mm long, and *ca.* 0.35 mm thick) were cut from the melt-pressed films quenched from various T_{iso} (180, 230 and 270 °C) by liquid nitrogen after the 2 hours isothermal treatment. The crystallinity was as low as 6–8% for the quenched films (ESI, Table S1†). The specimens were stretched to break with jaws moving symmetrically at a constant speed of 100 mm min^{-1} at ambient temperature (*ca.* 28 °C). Under the assumption that the sample volume kept a constant during the uniaxial elongation, the true strain was used as a measurement for the deformation, according to Strobl and co-workers.[57,58] With the thickness, width, and marked distance between the specific points of the initial (W_o, T_o, b_o) and stretched (W, T, b) specimens, the true stress (σ), draw ratio (λ), and true stress (ε_H) can be defined as follows (where F is the detected force):

$$\sigma = \frac{Fb}{W_o b_o T_o}\lambda = b/b_o\varepsilon_H = \ln\lambda$$

The measurement was repeated 3 times for each condition.

Results and discussion

Temperature effect on the microstructure of PEBAs

To reveal the time effect on the microstructure of PEBA, the G' of P35D melt as a function of ω obtained before and after the isothermal treatment at various T_{iso} are shown in Fig. 2a and b, respectively. The typical terminal flow region can be seen at 170 and 190 °C since the scaling laws of $G' \sim \omega^{2.0}$ is validated, indicating that P35D has reached the thermodynamically homogenous in the temperature range of 170–190 °C.[22,24,59,60] However, G' has deviated the scaling law from 200 °C (the

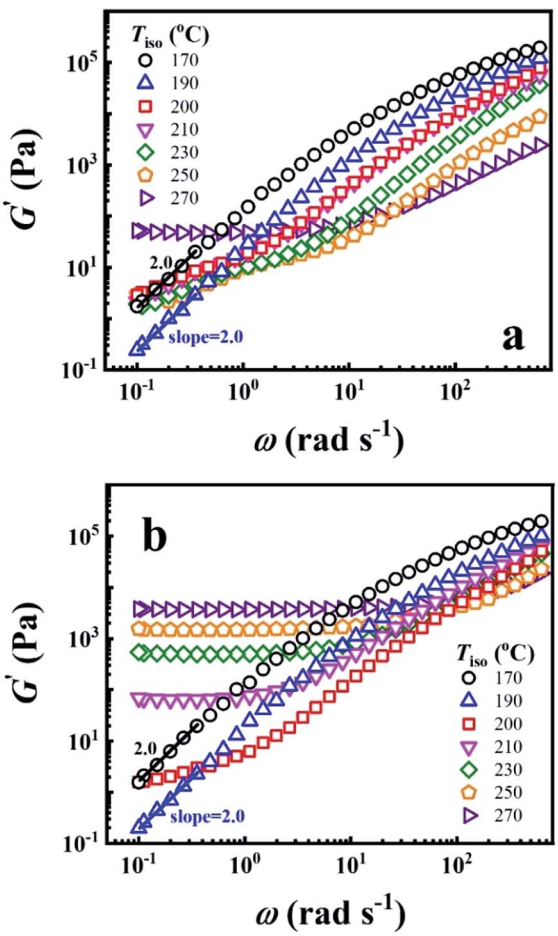

Fig. 2 Double Logarithmic plots of G' against ω (a) before and (b) after the 2 hours isothermal treatment at different T_{iso}.

deviation behavior was also seen for Pebax® 5533).[41] Furthermore, a short-range plateau is formed at low frequencies after the 2 hours isothermal process since 210 °C (Fig. 2b), suggesting that a certain network structure has been developed in P35D melt. When $T_{iso} \geq 210$ °C, the magnitude of G' and G'' increase rapidly with time during the isothermal process and G' eventually surpass G'' at low frequency (see ESI, Fig. S1†), whereas G' and G'' slightly decrease in the homogenous states (for example, in the temperature range of 170–190 °C). Fig. 2b shows that the magnitude of G' plateau was enhanced with the increasing T_{iso}, indicating the network structure becomes stronger and contributes a greater elastic property at higher temperatures. For the three studied PEBA copolymers with different PA12 content, the time effects on G' and G'' at high temperatures are similar, *i.e.*, a pronounced solid-like behavior ($G' \gg G''$) over the detected frequency range (ESI, Fig. S2†) can be observed after the isothermal treatment at 270 °C for all the three cases. It is probably ascribed by the chemical crosslinking network. The existence of the crosslinking network in these PEBA copolymers after the isothermal at 270 °C was confirmed by the swelling experiment with the *N*,*N*-dimethylformamide (DMF) solvent (see ESI, Fig. S3†), some swollen and insoluble matters were seen by the naked eyes for the isothermal-treated films, whereas the raw pellets were all apparent dissolved in DMF. The increased intrinsic viscosity with T_{iso} also indicates the occurrence of crosslinking reaction (ESI, Table S2†). Based on the results, it is supposed that the polyamide crosslinking reaction can be ignored within the 2 hours rheological measurement because of the extremely low reaction rate (the time has a very weak effect on the G' increase) when $T_{iso} \leq 210$ °C. However, due to the high reaction rate at 270 °C, the content of crosslinking network is high enough that it cannot be ignored after the 2 hours isothermal treatment and leads to an evident G' plateau.

FTIR result provides another piece of evidence for the existence of crosslinking structure. Fig. 3 shows the two FTIR spectra of the P35D hot-pressed films with and without the 2 hours isothermal treatment at 270 °C. It was found that the band position and relative height of the bands related to amide group between the two spectra are different, *i.e.*, the crosslinking network is closely associated with the amide groups. With the crosslinking network, the amide A band (stretching band of N–H group) at 3295 cm^{-1} shifts toward higher wavenumbers, indicating weakening strength of the hydrogen bonding. Moreover, some differences at 3100, 1483, 1223, 941, and 680 (amide V) cm^{-1} were also observed, which is consistent with our previous result in PA1012 homopolymer.[48] Different from the PA1012 homopolymer, the amide II band (stretching band of C–N group and deformation vibration band of N–H group) at 1560 cm^{-1} shifts to lower wavenumber with the crosslinking network. For the film with crosslinking network (blue curve in Fig. 3), the absorbances of the bands at 2918 and 2859 cm^{-1} (corresponding to the $-CH_2-$ asymmetrical and symmetrical stretching modes, respectively) are saturated due to the thicker film-thickness, lead to the not sharp bands.

It was reported that the secondary amine groups (R_1–NH–R_2) are obtained by the reaction between the end groups of various polyamide homopolymers (known as diamine coupling) and act as branch points that react with carboxyl groups to form the branched structures (ESI, Scheme S1†).[49,50] For polyamide melts at high temperature, the depolymerization of polyamide chains can also occur due to the ammonolysis reactions, and the depolymerized segments with $-CONH_2$ end-group can further reacts with the secondary amine group to form the crosslinking structures.[61] In other words, the chain scission and crosslinking are probably occurring simultaneously. As a result, both the end groups and the amide group in the repeating unit of polyamide chains can act as a crosslinking point. Based on the above reaction mechanisms, we propose a possible mechanism for the crosslinking reaction of PEBA elastomers as Scheme 1. The crosslinking structure established by the amide group of the repeating units of PA12 HS provides an additional elasticity for the studied PEBA elastomers. Although the proposed mechanism seems reasonable according to the literature, more research is needed to clarify it.

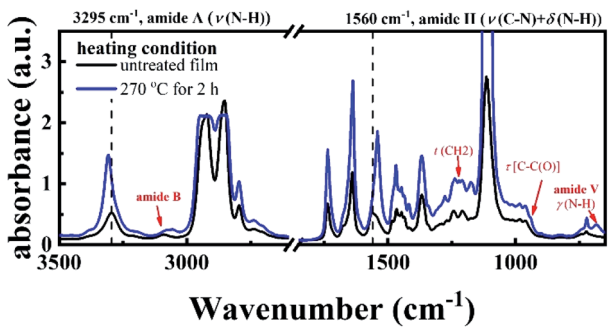

Fig. 3 The FTIR spectra of the P35D films, including the untreated film without any isothermal treatment (black line) and the film quenched from 270 °C after the 2 hours isothermal treatment in a vacuum chamber (blue line). The differences between curves are indicated by the dash lines and red arrows.

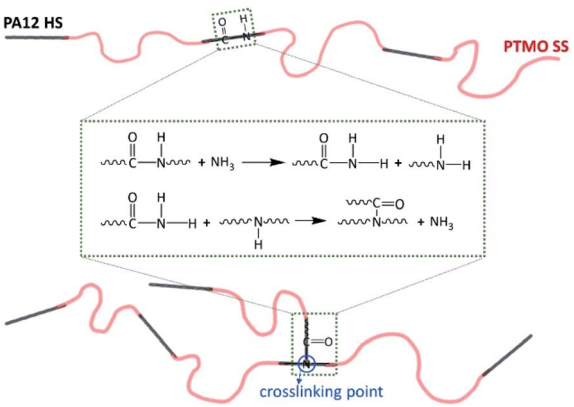

Scheme 1 Illustration of the possible crosslinking mechanism for the studied PEBA elastomers. The amide group in the repeating unit of PA12 HS first undergoes ammonolysis reactions with the ammonia molecules obtained by the reaction between end groups (known as diamine coupling), and then reacts with secondary amine group which acts as a crosslinking point to form a branched structure.

It should be noted that the scaling law of $G' \sim \omega^{2.0}$ is invalidated at 200 °C (Fig. 2a), and the crosslinking reaction can be ignored at T_{iso} < 210 °C due to the extremely low reaction rate. According to the AFM images of Pebax® 5533 films quenched from the melt state,[41] the microphase separation can be developed within several minutes. Therefore, it's reasonable the P35D melt is not homogenous one-phase but microphase separated at 200 °C, the physical microphase structure is strong enough to lead to the deviation of $G' \sim \omega^{2.0}$. However, the microstructure of P35D melt may be dominated by the crosslinking network after the isothermal at 200 °C for an infinite period of time, even if the reaction rate is extremely low.

In block copolymers, it's well known that the microphase separation can lead to the deviation of the scaling law of $G' \sim G''^{2.0}$ in the Han-plot, for which is an important means of detecting the existence of microphase separation.[2,21–23,27,60] Fig. 4 shows the Han-plots obtained from P25D, P35D, and P40D after the 2 hours isothermal treatment at various T_{iso}. It was found that the homogenous criterion of $G' \sim G''^{2.0}$ is only valid in 170–190 °C for P35D. Considering that no G' plateau is detected in the Han-plots and the magnitude of G' does not increase significantly with time (see ESI, Fig. S1†), P25D and P40D are considered to be microphase separated at 170 °C. At higher temperatures, such as 210–270 °C, the evident crosslinking network has been developed in all the three copolymers.

Ternary microstructure domains of PEBA upon heating

From the rheological results, there should be two transition temperatures in PEBA copolymers: the microphase separation temperature (transition from homogenous to microphase-separated state) and the initial temperature at which the crosslinking network begins to dominate (denoted as T_{cross}). The microphase separation is a reversible thermodynamic behavior, the state is a function of temperature, while the crosslinking network is an irreversible evolution. Determination of these two transition temperatures is of great significance for controlling the microstructure and also the rheological properties.

Due to the existence of crosslinking network, the microphase separation transition temperature cannot be determined precisely by the typical means such as Han-plot and SAXS in our system. The microphase separation originates from the interaction between the hard- and soft-segments, the apparent homogenous morphology and the possible short-range order structures may exist in the disorder state of block copolymers.[2] In contrast, the long-range order structures are formed in the microphase separation region in the phase diagram. In other words, the microphase separation temperature can be defined by the relative phase domain size. Herein, the transition temperature can be analog with the binodal temperature in polymer blends, which are induced by the concentration fluctuation. Therefore, the T_b of P35D can be estimated by using the Ajji and Chopin's method.[54–56] Fig. 5a shows the temperature dependence of G' and G'' with various heating rates. These curves merged well at low temperatures, where the homogenous criterion was satisfied. For each heating traces, the T_b was determined by the G' minimum[62] at where G' starts to upturn because of the strong enough concentration fluctuation. Meanwhile, T_s was determined from the extrapolation of the linear regression on the x-axis of the plots of $(G''^2/G'T)^{2/3}$ *versus* the reciprocal of temperature $1/T$ at a given heating-rate (shown in ESI, Fig. S4†) according to the Ajji and Chopin's model. Noted that T_s was obtained with the experimental data at the apparent homogenous region ($T < T_b$) for ensuring accuracy. Because the microphase separation is a time-dependent behavior, the heating rate effect on T_b and T_s should be considered. The good linear relationships for T_b and T_s *versus* heating rate are seen in Fig. 5b, the transition temperatures at equilibrium state (denoted as T_b° and T_s°) are determined to be 200.8 and 229.6 °C, respectively, by the extrapolation on the y-axis. Therefore, the PEBA copolymers exhibit an LCST-type phase diagram, also called lower disorder-to-order transition behavior. It's reminded

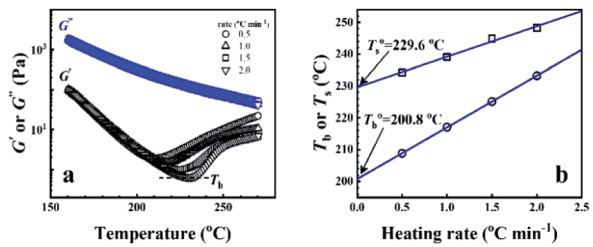

Fig. 5 (a) Temperature dependence of dynamic moduli obtained from P35D melt with various heating rates. T_b is determined by the temperature of G' minimum for each curve. (b) Effect of heating rate on the determined T_b and T_s. The extrapolation values on the y-axis represent the temperatures at equilibrium state, denoted as T_b° and T_s°.

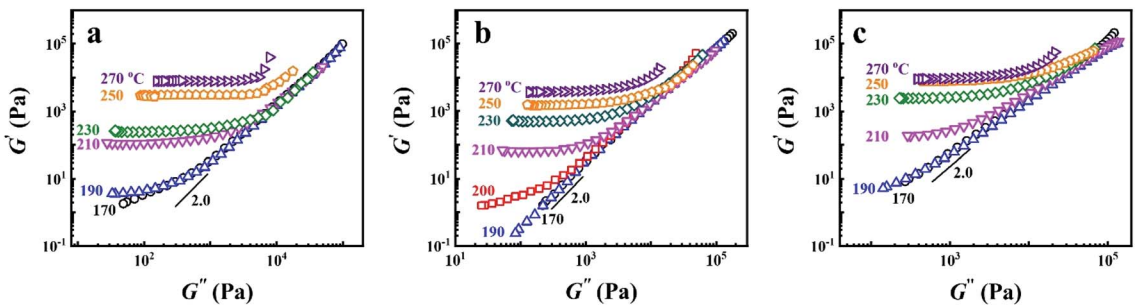

Fig. 4 Han-plots obtained from (a) P25D, (b) P35D, and (c) P40D melts after the 2 hours isothermal treatment at various T_{iso} from 170–270 °C.

that the applied SAOS may shift the binodal line in the phase diagram and induce a temperature-gap with the quiescent state, the gap is smaller at the lower frequency[63,64] In this work, all the temperature sweep measurements were performed at ω of 0.5 rad s^{-1}, thus, the T_b° is considered to be reliable and close to that obtained at the quiescent state. The obtained T_b° is consistent with the Han-plot result that the microphase separation has been developed in P35D at 200 °C. Although the phase diagram of Pebax® elastomers has not yet been constructed, it may be a dynamic asymmetric system because there is a considerable gap between $T_{c,HS}$ and $T_{c,SS}$ (Table 1).

In our system, once the microphase separation behavior occurs, it's difficult to distinguish the contribution from the crosslinking process on dynamic moduli in the initial stage. Moreover, the crosslinking reaction is time-dependent with a slow rate at lower temperatures. Therefore, the T_{cross} can only be approximately determined by the following experiments: one fresh sample was firstly heated to 170 °C and hold isothermal for 2 hours, then quickly jumped to various T_{iso} and hold isothermal for 2 hours, finally cooled back to 170 °C to check whether the microstructure is recoverable. Fig. 6a clearly shows that G' of P35D returned to the equilibrium value (black color) at 170 °C within 2 hours in the case of $T_{iso} = 190$ °C (below T_b°), the reversible behavior indicates it's the homogenous state at 190 °C which is in good agreement with the Han-plots (Fig. 4b). In $T < T_b^\circ$, the rheological properties are only affected by the chain entanglement. Although G' shows an upward trend at T_{iso} of 203 °C within two hours, G' eventually returns to the equilibrium value at 170 °C, implying that the content of crosslinking structure is so low that can be ignored within the measurement at 203 °C. On the other hand, the G' cooled down from T_{iso} of 207 °C remained almost constants and three-folds higher than the equilibrium value at 170 °C, the considerable gap indicates the microstructure has been dominant by the crosslinking structure. It can be concluded that the exactly T_{cross} is in the range of 203–207 °C. When $T_{iso} > T_{cross}$, the crosslinking network develops rapidly, and becomes the dominant factor in determining the microstructure and rheological properties within 2 hours.

Based on our experiments, the microstructure evolution of PEBAs upon heating can be divided into ternary domains: the apparent homogenous, microphase separation, and crosslinking domains, by the determined T_b° and T_{cross}. Taking P35D as an example, it is apparent homogenous state (the hard and soft segments are compatible at the molecular level) in the temperature range of $T_{m,HS} < T < T_b^\circ$. Meanwhile, the rheological properties and microstructure are reversible and depending on the temperature. In the range of $T_b^\circ \leq T_{iso} < T_{cross}$, a microphase-separated P35D melt was obtained after the 2 hours isothermal treatment, the content of crosslinking network is negligible due to the slow reaction rate. The microstructure is mainly affected by the microphase separation, the equilibrium state at a given temperature can be reached over a period of time. However, once the P35D melt was heated to temperatures

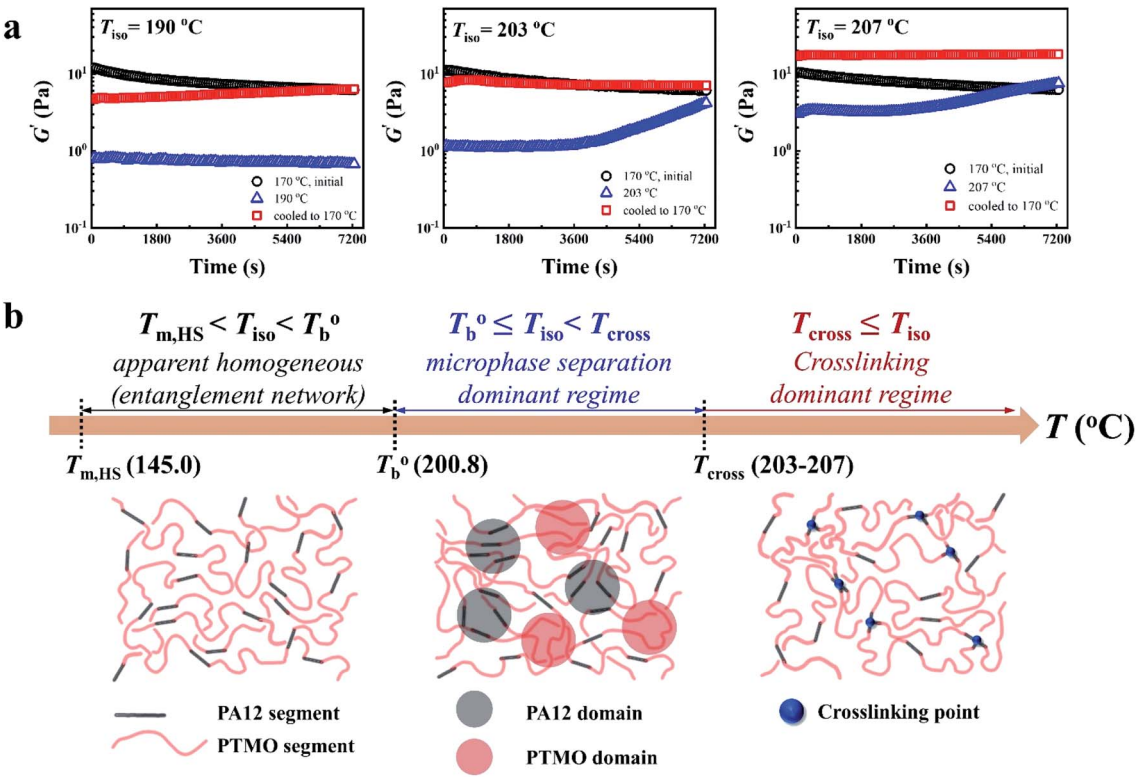

Fig. 6 (a) The effect of thermal history (isothermal treatment at various T_{iso}) on the magnitude of G' of P35D with respect to time at 170 °C. The applied ω is 0.1 rad s^{-1}. (b) Schematic representation of the microstructure domains in PEBA copolymers at the respective temperature regions. The critical temperatures of P35D are indicated on the temperature axis.

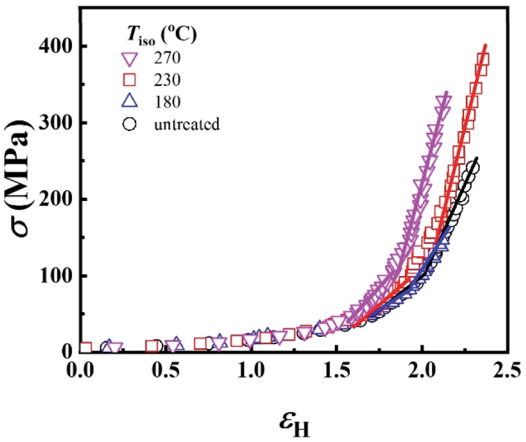

Fig. 7 True stress–strain curves of P35D, including the untreated sample without any thermal-treatment and the samples after the 2 hours isothermal at various T_{iso}: 180, 210, and 270 °C. The applied crosshead speed is 100 mm min^{-1}. The solid lines at large strain are used to guide the eyes.

Table 2 Tensile properties of the P35D after the 2 hours isothermal treatment at various T_{iso}

T_{iso} (°C)	Young's modulus (MPa)	Strain-at-break (%)	Stress-at-break (MPa)
Untreated	5.0 ± 0.3	228.7 ± 1.4	222.8 ± 41.7
180	4.8 ± 0.1	219.0 ± 11.5	270.6 ± 48.5
230	5.5 ± 0.2	235.1 ± 0.7	316.4 ± 57.7
270	5.2 ± 0.2	211.7 ± 10.4	326.3 ± 60.2

above T_{cross}, the content of crosslinking network (or crosslinking density) increases significantly, and becomes the dominant factor within a short period, resulting in the irreversible evolutions in microstructure. As presented, the rheological properties are also irreversible with temperature/time in this temperature domain. Not only PEBA copolymers, the reported irreversible effect of thermal history on the rheological properties in the TPU elastomers[20] can also be explained by this mechanism.

Unfortunately, no intensity peak associated with the long-range ordered structures was detected after the isothermal-treatment in the P35D's SAXS experiments (ESI, Fig. S5†), even in the microphase-separated domains. It may be caused by the poor contrast of electron cloud density between the hard- and soft-segments. In addition, no evident long-range order structure was observed by the TEM technique for the ultra-thin sections of P35D films quenched from T_{iso} above T_b° after the 2 hours isothermal process (shown in ESI, Fig. S6†). There are two possibilities: the first one is that interdomain distance is too short to be clearly seen. The interdomain distance can be as small as serval nanometers to tens of nanometers for Pebax® elastomers,[41,65] which is much smaller than the specimen thickness (*ca.* 90 nm). Therefore, the obtained ultra-thin section may contain tens of layers of this kind of structure, resulting in the homogenous-like morphology. The other possibility is that the crosslinking network inhibits the formation of the long-range order structures at $T > T_{cross}$. For the three studied elastomers, the lower $\Delta H_{m,HS}$ and $\Delta H_{c,HS}$ of the treated films after the isothermal process at 270 °C compared to the respective raw pellets implies that the presence of crosslinking network can reduce the regularity of the polymer chains. In other words, the chain mobility of P35D melt is probably restricted by the formed crosslinking structures.

Effect of the crosslinking network on mechanical properties

In the last section, the effect of the crosslinking network on the mechanical properties of P35D at room temperature is investigated by comparing the quenched samples that have been isothermally treated at different T_{iso}. The true stress–strain curves of P35D after the isothermal-treatment at various T_{iso} are shown in Fig. 7, the typical elastomer behavior was seen for the untreated sample without any isothermal treatment (black circle). In the case of T_{iso} of 180 °C (lower than T_b°), the curve (blue triangle) was almost identified with the untreated one because of the reversible entanglement network, whereas the steeper increase trend of stress *versus* strain was detected in the case of T_{iso} of 230 and 270 °C (both of them are higher than T_{cross}). From Fig. 2b, the magnitude of the G' plateau obtained from T_{iso} of 270 °C is *ca.* 7-fold of that from 230 °C, suggesting that the crosslinking density at 270 °C is several times higher than that of 230 °C. The stronger network provides an additional elasticity. Compared with the untreated sample, the stress-at-break was enhanced to 326.3 ± 60.2 MPa at T_{iso} of 270 °C, as 1.47-fold of that of the untreated sample. It should be noted that the strain-hardening phenomenon becomes more pronounced as the crosslinking density increases. Our previous work has demonstrated that the strain-hardening phenomena in PEBA copolymers is related to the strain-induced crystallization of PTMO segments and the orientations of molecular segments.[39] Our true stress–strain curves implied that the existence of the crosslinking network has a considerable influence on the strain-induced crystallization of the PTMO segment at the large deformation for PEBA elastomers, although the mechanical properties do not show a significant difference with the increasing T_{iso} (Table 2).

Conclusions

In this work, the microstructure evolution of the poly(ether-*b*-amide) segmental copolymer upon heating was investigated *via* rheological measurement. Based on our experiments, the crosslinking network by the inherent crosslinking reaction in the polyamide segments is confirmed to be formed, and dominates the microstructure of the three studied PEBA copolymers at temperatures higher than T_{cross}. With the obtained T_b° and T_{cross}, the microstructure evolution of PEBA upon the heating process can be classified into ternary domains, they are the homogenous ($T_{m,HS} < T < T_b^\circ$), microphase separated ($T_b^\circ \leq T < T_{cross}$), and the crosslinking ($T_{cross} < T$) domains. Our experiments have demonstrated that when P35D melt is once heated above T_{cross} (*ca.* 58–62 °C higher than $T_{m,HS}$ in P35D), the

content of the crosslinking network increases rapidly with time and temperature, leading to an irreversible and non-negligible influence on the rheological, crystallization, and mechanical properties. To the best of our knowledge, the present work is the first to systematically explore the microstructure evolution from the apparent homogenous to crosslinked state in PEBA copolymers.

Determination of the critical temperatures ($T_{m,HS}$, T_b° and T_{cross}) is important for regulating the microstructure and studying PEBA's structure–property relationship. It should be noted that these critical temperatures are depending on the content of PA component. For example, the $T_{m,HS}$ of PEBA increases with the content of polyamide segment, it is possible to even higher than T_b°. In that case, no homogenous state can be obtained. Although this work has demonstrated the competition between the microphase separation and crosslinking structures for the microstructure of PEBA, the mechanism is still not well understood from the molecular level viewpoint.

These results provide a deep understanding of the microstructure evolution of the PEBA elastomers. Further investigations of the effects of microstructure evolution and chemical crosslinking on the crystallization behaviors of PEBA are undertaking in our lab, and the results will be reported in the near future.

Conflicts of interest

There are no conflicts to declare.

Acknowledgements

This work was financially supported by the National Natural Science Foundation of China (51820105005) and the STS Program of Chinese Academy of Sciences (KFJ-STS-QYZX-113).

Notes and references

1 G. H. Fredrickson and E. Helfand, *J. Chem. Phys.*, 1987, **87**, 697–705.
2 N. Sakamoto, T. Hashimoto, C. D. Han, D. Kim and N. Y. Vaidya, *Macromolecules*, 1997, **30**, 1621–1632.
3 F. Kayser, G. Fleury, S. Thongkham, C. Navarro, B. Martin-Vaca and D. Bourissou, *Macromolecules*, 2018, **51**, 6534–6541.
4 M. Qiu, X. Z. Zhao, D. P. Liu and C. J. He, *RSC Adv.*, 2015, **5**, 17851–17861.
5 K. Takano, T. Nyu, T. Maekawa, T. Seki, R. Nakatani, T. Komamura, T. Hayakawa and T. Hayashi, *RSC Adv.*, 2020, **10**, 70–75.
6 L. Leibler, *Macromolecules*, 1980, **13**, 1602–1617.
7 P. He, W. Shen, W. Yu and C. Zhou, *Macromolecules*, 2014, **47**, 807–820.
8 M. W. Matsen and M. Schick, *Phys. Rev. Lett.*, 1994, **72**, 2660–2663.
9 R. H. Colby, *Curr. Opin. Colloid Interface Sci.*, 1996, **1**, 454–465.
10 H. E. Park, J. M. Dealy, G. R. Marchand, J. Wang, S. Li and R. A. Register, *Macromolecules*, 2010, **43**, 6789–6799.
11 L. Zhu, Y. Chen, A. Zhang, B. H. Calhoun, M. Chun, R. P. Quirk, S. Z. D. Cheng, B. S. Hsiao, F. Yeh and T. Hashimoto, *Phys. Rev. B: Condens. Matter Mater. Phys.*, 1999, **60**, 10022–10031.
12 S. Velankar and S. L. Cooper, *Macromolecules*, 1998, **31**, 9181–9192.
13 S. Velankar and S. L. Cooper, *Macromolecules*, 2000, **33**, 382–394.
14 W. Gabriëlse, M. Soliman and K. Dijkstra, *Macromolecules*, 2001, **34**, 1685–1693.
15 P. Ping, W. Wang, X. Chen and X. Jing, *J. Polym. Sci., Part B: Polym. Phys.*, 2007, **45**, 557–570.
16 L. L. Wang, X. Dong, P. Zhu, X. Q. Zhang, X. R. Liu and D. J. Wang, *Eur. Polym. J.*, 2017, **90**, 171–182.
17 L. L. Wang, X. Dong, P. Zhu, X. Q. Zhang and D. J. Wang, *Acta Polym. Sin.*, 2017, **5**, 752–760.
18 R. Y. Wang, X. S. Guo, B. Fan, S. F. Zou, X. H. Cao, Z. Z. Tong, J. T. Xu, B. Y. Du and Z. Q. Fan, *Macromolecules*, 2018, **51**, 2302–2311.
19 R. Y. Wang, J. Huang, X. S. Guo, X. H. Cao, S. F. Zou, Z. Z. Tong, J. T. Xu, B. Y. Du and Z. Q. Fan, *Macromolecules*, 2018, **51**, 4727–4734.
20 P. J. Yoon and C. D. Han, *Macromolecules*, 2000, **33**, 2171–2183.
21 M. B. Kossuth, D. C. Morse and F. S. Bates, *J. Rheol.*, 1999, **43**, 167–196.
22 S. Choi, N. Y. Vaidya, C. D. Han, N. Sota and T. Hashimoto, *Macromolecules*, 2003, **36**, 7707–7720.
23 K. Almdal, F. S. Bates and K. Mortensen, *J. Chem. Phys.*, 1992, **96**, 9122–9132.
24 J. H. Rosedale and F. S. Bates, *Macromolecules*, 1990, **23**, 2329–2338.
25 F. S. Bates, *Science*, 1991, **251**, 898–905.
26 F. S. Bates, *Macromolecules*, 1984, **17**, 2607–2613.
27 C. D. Han, J. Kim and J. K. Kim, *Macromolecules*, 1989, **22**, 383–394.
28 J. P. Sheth, J. Xu and G. L. Wilkes, *Polymer*, 2003, **44**, 743–756.
29 D. J. Arriola, E. M. Carnahan, P. D. Hustad, R. L. Kuhlman and T. T. Wenzel, *Science*, 2006, **312**, 714–719.
30 S. Y. Dong, P. Zhu, J. G. Liu, D. J. Wang and X. Dong, *Acta Polym. Sin.*, 2019, **50**, 189–198.
31 S. Fakirov, *Handbook of Condensation Thermoplastic Elastomer*, WiLEY-VCH, Weinheim, 2005.
32 F. Zuo, C. G. Alfonzo and F. S. Bates, *Macromolecules*, 2011, **44**, 8143–8153.
33 S. Velankar and S. L. Cooper, *Macromolecules*, 2000, **33**, 395–403.
34 B. Tavernier, J. Mewis, P. Van Puyvelde, M. Takenaka, B. Ernst and T. Hashimoto, *Polym. Eng. Sci.*, 2008, **48**, 2418–2425.
35 Y. Y. Cao, P. Zhu, Z. F. Wang, Y. Zhou, H. M. Chen, A. J. Müller, D. J. Wang and X. Dong, *Polym. Cryst.*, 2018, **1**, e100121.

36 P. Zhu, X. Dong, Y. Y. Cao, L. L. Wang, X. R. Liu, Z. F. Wang and D. J. Wang, *Eur. Polym. J.*, 2017, **93**, 334–346.
37 H. S. Lee, H. D. Park and C. K. Cho, *J. Appl. Polym. Sci.*, 2000, **77**, 699–709.
38 B. B. Sauer, R. S. McLean, D. J. Brill and D. J. Londono, *J. Polym. Sci., Part B: Polym. Phys.*, 2002, **40**, 1727–1740.
39 P. Zhu, X. Dong and D. J. Wang, *Macromolecules*, 2017, **50**, 3911–3921.
40 P. Zhu, X. Dong, M. M. Huang, L. L. Wang, S. X. Qi and D. J. Wang, *J. Polym. Sci., Part B: Polym. Phys.*, 2018, **56**, 855–864.
41 I. K. Yang and P. H. Tsai, *J. Polym. Sci., Part B: Polym. Phys.*, 2005, **43**, 2557–2567.
42 R. Hill, *Chem. Ind.*, 1954, **36**, 1083–1089.
43 G. Meacock, *J. Appl. Chem.*, 1954, **4**, 172–177.
44 I. Goodman, *J. Polym. Sci.*, 1955, **17**, 587–590.
45 L. H. Peebles and M. W. Huffman, *J. Polym. Sci., Part A-1: Polym. Chem.*, 1971, **9**, 1807–1822.
46 G. Filippone, S. C. Carroccio, R. Mendichi, L. Gioiella, N. T. Dintcheva and C. Gambarotti, *Polymer*, 2015, **72**, 134–141.
47 J. Zhang and A. Adams, *Polym. Degrad. Stab.*, 2016, **134**, 169–178.
48 X. R. Liu, Y. Wang, L. Y. Liu, X. Dong and D. J. Wang, *Chin. J. Polym. Sci.*, 2020, **38**, 993–998.
49 R. E. Kirk, D. F. Othmer, J. I. Kroschwitz and M. Howe-Grant, *Encyclopedia of Chemical Technology*, ed. K. Othmer, Wiley VCH, 1991, vol. 19, pp. 224–229.
50 V. Korshak and T. Frunze, *Synthetic Hetero-Chain Polyamides*, IPST, Israel, 1964.
51 D. W. Janes, V. Chandrasekar, S. E. Woolford and K. B. Ludwig, *Macromolecules*, 2017, **50**, 6137–6148.
52 Y. Song, H. Yamamoto and N. Nemoto, *Macromolecules*, 2004, **37**, 6219–6226.
53 M. E. Rezac and T. John, *Polymer*, 1998, **39**, 599–603.
54 A. Ajji and L. Choplin, *Macromolecules*, 1991, **24**, 5221–5223.
55 M. Pakravan, M. C. Heuzey and A. Ajji, *Macromolecules*, 2012, **45**, 7621–7633.
56 J. Khademzadeh Yeganeh, F. Goharpey and R. Foudazi, *Macromolecules*, 2010, **43**, 8670–8685.
57 R. Hiss, S. Hobeika, C. Lynn and G. Strobl, *Macromolecules*, 1999, **32**, 4390–4403.
58 Y. Men and G. Strobl, *Macromolecules*, 2003, **36**, 1889–1898.
59 C. D. Han and J. Kim, *J. Polym. Sci., Part B: Polym. Phys.*, 1987, **25**, 1741–1764.
60 C. D. Han, D. M. Baek and J. K. Kim, *Macromolecules*, 1990, **23**, 561–570.
61 L. H. Peebles Jr and M. W. Huffman, *J. Polym. Sci., Part A: Polym. Chem.*, 1971, **9**, 1807–1822.
62 W. Liu, X. Dong, F. S. Zou, J. Yang, D. J. Wang and C. C. Han, *Polymer*, 2014, **55**, 2744–2750.
63 F. S. Zou, X. Dong, D. Lin, W. Liu, D. J. Wang and C. C. Han, *Polymer*, 2012, **53**, 4818–4826.
64 F. S. Zou, X. Dong, W. Liu, J. Yang, D. Lin, A. Liang, W. Li and C. C. Han, *Macromolecules*, 2012, **45**, 1692–1700.
65 R. S. McLean and B. B. Sauer, *Macromolecules*, 1997, **30**, 8314–8317.